Evolution of the Jahn−Teller Distortion of MnO_6 Octahedra in $RMnO_3$ Perovskites (R = Pr, Nd, Dy, Tb, Ho, Er, Y): A Neutron Diffraction Study

J. A. Alonso,* M. J. Martínez-Lope, and M. T. Casais

Instituto de Ciencia de Materiales de Madrid, CSIC, Cantoblanco, E-28049 Madrid, Spain

M. T. Fernández-Díaz

Institut Laue-Langevin, B.P. 156, F-38042 Grenoble Cedex 9, France

Received August 2, 1999

Stoichiometric $RMnO_3$ perovskites have been prepared in the widest range of R^{3+} ionic sizes, from $PrMnO_3$ to $ErMnO_3$. Soft-chemistry procedures have been employed; inert-atmosphere annealings were required to synthesize the materials with more basic R cations (R = Pr, Nd), in order to minimize the unwanted presence of Mn^{4+}. On the contrary, annealings in O_2 flow were necessary to stabilize the perovskite phases for the last terms of the series, $HoMnO_3$, $ErMnO_3$, and $YMnO_3$, thus avoiding or minimizing the formation of competitive hexagonal phases with the same stoichiometry. The samples have been investigated at room temperature by high-resolution neutron powder diffraction to follow the evolution of the crystal structures along the series. The results are compared with reported data for $LaMnO_3$. The distortion of the orthorhombic perovskite (space group *Pbnm*), characterized by the tilting angle of the MnO_6 octahedra, progressively increases from Pr to Er due to simple steric factors. Additionally, all of the perovskites show a distortion of the MnO_6 octahedra due to the orbital ordering characteristic of the Jahn−Teller effect of Mn^{3+} cations. The degree of orbital ordering slightly increases from La to Tb and then remains almost unchanged for the last terms of the series. The stability of the crystal structure is also discussed in light of bond-valence arguments.

I. Introduction

$LaMnO_3$ perovskite has been extensively studied in the past years, since it is the parent compound of the family of oxides $La_{1-x}A_xMnO_3$ (A = alkaline earth), showing interesting properties such as colossal magnetoresistance or charge-ordering.[1,2] In this family, the replacement of La for divalent A cations oxidizes Mn^{3+} to Mn^{4+}, introducing holes in the Mn 3d band and giving rise to metallic and/or ferromagnetic behavior. Even in the absence of chemical doping, $LaMnO_3$ shows the ability to accommodate the so-called "oxidative nonstoichiometry",[3−5] which also involves the partial oxidation of some Mn^{3+} to Mn^{4+} cations in samples of global composition $LaMnO_{3+\delta}$. In fact, the insertion of excess oxygen is not possible in the perovskite structure, and the nonstoichiometry is incorporated via cation vacancies.[6−9] The actual crystallographic formula of such compositions should be written as $La_{1-x}Mn_{1-x}O_3$, with $x = \delta/(3 + \delta)$. The formation of these defective materials is simply achieved by annealing the samples in air or O_2 atmosphere,[10] given the ease of the oxidation process $Mn^{3+} \rightarrow Mn^{4+} + 1\ e^-$. The presence of mixed $Mn^{3+} - Mn^{4+}$ valences gives rise to a double-exchange mechanism similar to that observed in A-substituted perovskites, increasing drastically the electrical conductivity and inducing ferromagnetic-like behavior with reentrant spin-glass character.[11,12]

Nevertheless, the stoichiometric $LaMnO_{3.00}$ perovskite, containing 100% Mn^{3+}, is very interesting itself. The synthesis of this sample requires special conditions, involving annealings under inert atmosphere. The absence of a mixed Mn valence determines the insulating character of this phase; at the same time the Jahn−Teller (JT) character of Mn^{3+} ($t_{2g}^3e_g^1$) with a single e_g electron with orbital degeneracy is responsible for the static JT deformation observed at room temperature (RT), [13−15] leading to an antiferrodistorsive orbital ordering evidenced by the spatial distribution of the observed Mn−O bond lengths. At low temperatures the breakdown of the 2-fold degeneracy of the e_g orbitals stabilizes a layered A-type antiferromagnetic (AF) structure (below $T_N = 130$ K).[16] Between 1.5 and 750 K

* Corresponding author. E-mail: ja.alonso@icmm.csic.es.

(1) Ramirez, A. P. *J. Phys: Condens. Matter* **1997**, *9*, 8171.
(2) Rao, C. N. R., Raveau, B., Eds. *Colossal magnetoresistance and other related properties in 3d oxides*; World Scientific: Singapore, 1998.
(3) Hauback, B. C.; Fjellvag H.; Sakai, N. *J. Solid State Chem.* **1996**, *124*, 43.
(4) Mahendiran, R.; Tiwary, S. K.; Raychadhuri, A. K.; Ramakrisnan, T. V.; Mahesh, R.; Raganvittal, N.; Rao, C. N. R. *Phys. Rew. B* **1996**, *53*, 3348.
(5) Rao, C. N. R.; Cheetham, A. K. *Science* **1996**, *272*, 369.
(6) Tofield, B. C.; Scott, W. R. *J. Solid State Chem.* **1974**, *10*, 183.
(7) Van Roosmalen, J. A. M.; Cordfunke, E. H. P.; Helmholdt, R. B.; Zandbergen, H. W. *J. Solid State Chem.* **1994**, *110*, 100.
(8) Van Roosmalen, J. A. M.; Cordfunke, E. H. P. *J. Solid State Chem.* **1994**, *110*, 106.
(9) Alonso, J. A.; Martínez-Lope, M. J.; Casais, M. T.; MacManus-Driscoll, J. L.; de Silva, P. S. I. P. N.; Cohen, L. F. *J. Mater. Chem.* **1997**, *7*, 2139.
(10) Alonso, J. A.; Martínez-Lope, M. J.; Casais, M. T. *Eur. J. Solid State Inorg. Chem.* **1996**, *33*, 331.
(11) De Silva, P. S. I. P. N.; Richards, F. M.; Cohen, L. F.; Alonso, J. A.; Martínez-Lope, M. J.; Casais, M. T.; Thomas, K. A.; MacManus-Driscoll, J. L. *J. Appl. Phys.* **1998**, *83*, 394.
(12) Ghivelder, L.; Abrego-Castillo, I.; Gusmão, M. A.; Alonso, J.A; Cohen, L. F. *Phys. Rev. B* **1999**, *60*, 12184.
(13) Elemans, J. B. A. A.; Van Laar, B.; Van der Veen, K. R.; Loopstra, B. O. *J. Solid State Chem.* **1971**, *3*, 238.
(14) Norby, P.; Andersen, I. G. K.; Andersen E. K.; Andersen, N. H. *J. Solid State Chem.* **1995**, *119*, 191.
(15) Rodríguez-Carvajal, J.; Hennion, M.; Moussa, F.; Moudden, A. H.; Pinsard, L.; Revcolevschi, A. *Phys. Rev.* B **1998**, *57*, R3189.
(16) Wollan, E. O.; Koeler, W. C. *Phys. Rev.* **1955**, *100*, 545.

10.1021/ic990921e CCC: $19.00
Published on Web 02/11/2000

the structure is orthorhombic, space group *Pbnm*; above $T_{JT} = 750$ K a structural phase transition takes place: there is no change in space group symmetry, although the lattice becomes metrically cubic and MnO_6 octahedra distortion almost disappears.[15] The observation of large thermal factors for oxygen indicates the presence of a underlying dynamical JT effect.

The behavior of other members of the $RMnO_3$ series (R = rare earth) has been much less studied. There are only a few reports[17,18] of the crystal structures of $PrMnO_{3+\delta}$ and $NdMnO_{3+\delta}$ (also showing oxidative nonstoichiometry, since Pr and Nd also exhibit a strongly basic character, suitable to stabilize Mn^{4+}), but accurate structural parameters of stoichiometric $RMnO_{3.00}$ for Pr, Nd, or smaller rare-earth cations have not been reported. Moreover, it is of great interest to study the evolution of the RT JT distortion of MnO_6 octahedra as the size of R^{3+} (and hence the degree of distortion of the perovskite) changes within the widest possible limits. A recent study of the structural changes of manganese perovskites under external pressure[19] has shown that the main effect of this external parameter is to open the Mn−O−Mn angles and to shorten the Mn−O bond lengths, leading to a less distorted perovskite structure with a larger tolerance factor. On the contrary, the effect of the "internal pressure" or "chemical pressure" introduced by the progressive reduction of the R^{3+} size is opposite to that of the external pressure, leading to an increase of the distortion of the perovskite with a closing of the Mn−O−Mn angles. Therefore the observed changes along the series $RMnO_3$ are complementary to the results obtained under external pressure.

In the aim to extend as much as possible the study of the highly distorted $RMnO_3$ perovskites, we have made an effort to reach the most distorted terms of the series, in order to perform an accurate neutron powder diffraction (NPD) structural study of the whole family. For rare-earth cations smaller than Tb^{3+} the orthorhombic perovskite structure for $RMnO_3$ is no longer the stable phase under ordinary synthetic conditions, since a hexagonal non-perovskite phase (space group $P6_3cm$) with the same stoichiometry strongly competes in stability. However, $HoMnO_3$ and $YMnO_3$ can be prepared as metastable phases by working under soft-chemistry conditions.[20−22] Quezel et al.[20] prepared $YMnO_3$ from the citrate method, and they studied its magnetic structure from low-resolution NPD data. This paper references a thesis by Szabo,[21] commenting on the possibility of preparation of $ErMnO_3$ and $HoMnO_3$ by citrates decomposition, although this work was not further published. Brinks et al.[22] explored different experimental conditions, claiming the preparation of 99% pure orthorhombic $YMnO_3$. Recently, $YMnO_3$ has also been obtained in thin film form by pulsed laser deposition techniques.[23] Based on the work of Brinks et al.,[22] we have developed a successful route to prepare Y, Ho, and Er oxides as pure (R = Ho) or major (R = Y, Er) perovskite phases.

On the other hand, the intermediate $SmMnO_3$, $EuMnO_3$, and $GdMnO_3$ have not been studied in the present work given the high neutron absorption cross section of the corresponding rare earths. However, the moderately absorbing $DyMnO_3$ has been successfully studied by collecting NPD data under special conditions. In this paper we report on the RT crystal structure of stoichiometric $RMnO_3$ perovskites for R = Pr, Nd, Dy, Tb, Ho, Y, and Er. The results are contrasted with the available data for $LaMnO_3$, and the evolution of the JT distortion of the MnO_6 octahedra is discussed.

Table 1. Compositional Characterization of the Last Terms of the Series, of Actual Stoichiometry $RMnO_{3+\delta}$

	Ho	Y	Er
δ	0.01	0.04	0.03
% Mn^{4+}	2.0	8.0	6.0
% hexag	0.0	11.7(7)	16.0(5)

[a] Oxygen content has been determined by thermal analysis under reducing conditions (±0.01 O per formula). The fraction of hexagonal phases (for R = Y, Er) has been obtained from the refinement of NPD data.

II. Experimental Section

$RMnO_3$ were prepared from citrate precursors obtained by soft-chemistry procedures. Stoichiometric amounts of analytical grade R_2O_3 (R = Pr, Nd, Tb, Dy, Ho, Er, and Y) and $MnCO_3$ were dissolved in citric acid, by adding several droplets of concentrated HNO_3 to favor the solution of rare-earth oxides. The citrate + nitrate solutions were slowly evaporated, leading to organic resins containing a random distribution of the involved cations at an atomic level. These resins were first dried at 120 °C and then slowly decomposed at temperatures up to 600 °C. All the organic materials and nitrates were eliminated in a subsequent treatment at 700 °C in air, for 12 h. This treatment gave rise to highly reactive precursor materials, amorphous to X-ray diffraction (XRD). For R = Pr, Nd, the precursors were treated at 1100 °C in a N_2 flow for 12 h. Annealing treatments in an inert atmosphere were necessary to avoid the formation of oxidized $Pr(Nd)MnO_{3+\delta}$ phases, containing a significant amount of Mn^{4+}. For R = Tb, Dy, the precursor powders were heated at 1000 °C in air for 12 h.

Considerable effort was devoted to increase the yield of the orthorhombic phases for R = Ho, Y, and Er, preventing or minimizing the stabilization of competitive hexagonal $RMnO_3$ phases. The following points were observed. (i) Particularly important is the previous formation of an amorphous product of decomposition of the citrates, at 700 °C: once the crystallization of the hexagonal phase is observed, subsequent thermal treatments do not drive the transformation to the orthorhombic phase. (ii) The atmosphere in which the decomposition takes place is a key factor: N_2 or air favors the formation of the hexagonal phase, whereas O_2 (1 atm) allows the increase of the yield of orthorhombic perovskite, as observed by Brinks et al.[22] However, the treatment under high oxygen pressures leads to the stabilization of the pyrochlore $R_2Mn_2O_7$, as also reported by these authors. [22] (iii) Finally, the heating rate was found to have a dramatic influence on the phase ratio, a slow heating allowing us to optimize the yield of the orthorhombic phase. In the final run, the amorphous precursors were heated in an O_2 flow from 600 to 900 °C in 12 h, and then held at 900 °C for 12 h. This procedure enabled the preparation of pure $HoMnO_3$ perovskite, but could not avoid the formation of minor amounts of hexagonal phases for the Y and Er compounds (as indicated in Table 1).

The products were initially characterized by laboratory XRD for phase identification and to assess phase purity. The oxygen content of the samples was determined by thermal analysis in reducing conditions (H_2/N_2 flow), through total reduction to MnO + R_2O_3. For the structural refinements NPD patterns were collected at room temperature at the D2B high-resolution neutron diffractometer of ILL-Grenoble. The high-resolution mode was used; a wavelength of 1.594 Å was selected from a Ge monochromator. The collection time was 3 h. For $DyMnO_3$ a good quality pattern could be collected, despite the absorbing nature of Dy, by using a vanadium double-walled hollow cylindrical sample holder (8 mm diameter) to minimize absorption effects. A longer counting time of 8 h was necessary. The NPD data were treated by the Rietveld[24] method, using the FULLPROF refinement program.[25] A pseudo-Voigt function was chosen to generate the line shape of the

(17) Cherepanov, V. A.; Barkhatova, L. Yu.; Petrov, A. N.; Voronin, V. I. *J. Solid State Chem.* **1995**, *118*, 53.
(18) Kamegasgira, N.; Miyazaki, I. *Mater. Res. Bull.* **1984**, *19*, 1201.
(19) Laukin, V.; Fontcuberta, J.; García-Muñoz, J. L.; Obradors, X. *Phys. Rev. B* **1997**, *56*, 10009.
(20) Quezel, S.; Rossat Mignod, J.; Bertaut, E. F. *Solid State Commun.* **1974**, *14*, 941.
(21) Szabo, G. Ph.D. Thesis, Lyon, 1969.
(22) Brinks, H. W.; Fjellvag, H.; Kjekshus, A. *J. Solid State Chem.* **1997**, *129*, 334.
(23) Salvador, P. A.; Doan, T.-D., Mercey, B.; Raveau, B. *Chem. Mater.* **1998**, *10*, 2592.

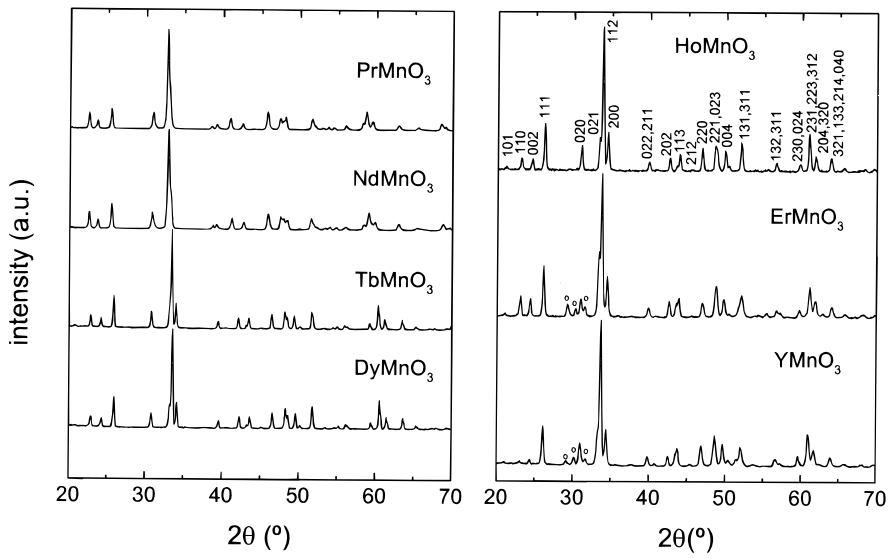

Figure 1. Laboratory XRD patterns for $RMnO_3$, R = Pr, Nd, Tb, Dy, Ho, Er, and Y. Small circles indicate the main reflections of the hexagonal $ErMnO_3$ and $YMnO_3$ impurity phases. The $HoMnO_3$ pattern is indexed in an orthorhombic unit cell with $a = 5.2572(1)$ Å, $b = 5.8354(1)$ Å, $c = 7.3606(1)$ Å.

Table 2. Unit-Cell, Positional, Thermal Parameters, and Reliability Factors for the Refinements of $RMnO_3$ Phases (R = La, Pr, Nd, Tb, Dy, Ho, Y, Er), in the Orthorhombic *Pbnm* Space Group, $Z = 4$, from NPD Data at 295 K[a]

		La	Pr	Nd	Tb	Dy	Ho	Y	Er
a (Å)		5.5367(1)	5.4491(1)	5.4170(5)	5.29314(5)	5.2785(1)	5.2572(1)	5.2418(3)	5.2262(2)
b (Å)		5.7473(1)	5.8129(2)	5.8317(5)	5.8384(1)	5.8337(1)	5.8354(1)	5.8029(3)	5.7932(3)
c (Å)		7.6929(2)	7.5856(2)	7.5546(7)	7.4025(1)	7.3778(1)	7.3606(1)	7.3643(4)	7.3486(3)
V (Å^3)		244.796(2)	240.278(5)	238.651(5)	228.760(6)	227.191(5)	225.807(4)	224.007(8)	222.49(1)
s		0.0377	0.0646	0.0737	0.0980	0.0999	0.1043	0.1016	0.1030
R	4c(x y $^1/_4$)								
x		0.9922(3)	0.9911(6)	0.9886(5)	0.9831(4)	0.9828(1)	0.9825(3)	0.9819(8)	0.9838(7)
y		0.0490(2)	0.0639(5)	0.0669(4)	0.0824(3)	0.0824(1)	0.0839(3)	0.0855(6)	0.0837(5)
B (Å^2)		0.34(2)	0.76(4)	0.72(4)	0.73(4)	0.41(1)	0.26(3)	0.87(8)	0.66(6)
Mn	4b($^1/_2$ 0 0)								
B (Å^2)		0.21(3)	0.63(6)	0.48(7)	0.84(7)	0.37(4)	0.39(6)	1.03(14)	1.01(12)
O1	4c(x y $^1/_4$)								
x		0.0745(3)	0.0834(4)	0.0878(5)	0.1038(5)	0.1092(3)	0.1113(4)	0.1093(9)	0.1114(7)
y		0.4874(3)	0.4819(4)	0.4790(5)	0.4667(4)	0.4642(3)	0.4622(4)	0.4660(8)	0.4646(7)
B (Å^2)		0.50(3)	0.75(4)	0.84(5)	0.67(5)	0.40(3)	0.38(4)	0.46(9)	0.54(8)
O2	8d(x y z)								
x		0.7256(2)	0.7151(3)	0.7141(4)	0.7039(4)	0.7028(3)	0.7013(3)	0.7005(7)	0.7003(6)
y		0.3066(2)	0.3174(3)	0.3188(3)	0.3262(3)	0.3276(3)	0.328183)	0.3266(6)	0.3266(5)
z		0.0384(2)	0.0430(2)	0.0450(3)	0.0510(2)	0.0521(2)	0.0534(2)	0.0520(5)	0.0542(4)
B (Å^2)		0.43(3)	0.76(3)	0.70(3)	0.86(3)	0.59(2)	0.45(3)	0.90(7)	0.92(6)
reliability factors									
χ^2		2.35	2.00	2.23	1.43	1.58	1.46	1.22	1.27
R_p (%)		8.98	4.19	4.14	2.33	2.43	3.82	4.60	2.89
R_{wp} (%)		9.04	5.28	5.16	2.95	3.02	4.78	5.85	3.68
R_1 (%)		5.16	5.31	5.70	6.30	3.27	6.20	6.68	5.49

[a] Data for La are taken from ref 15. The strain parameter is defined as $s = 2(b - a)/(a + b)$.

diffraction peaks. No regions were excluded in the refinement. For R = Y and Er, minor amounts of hexagonal $RMnO_3$ were detected in the patterns. Then, the profile refinement of the mixture was performed. In the final run the following parameters were refined: scale factor(s), background coefficients, zero-point error, unit-cell parameters, pseudo-Voigt corrected for asymmetry parameters, phase fraction(s), positional coordinates, and isotropic thermal factors. The unit-cell parameters and the coefficients to fit the peak shape for the secondary phases were also refined.

III. Results and Discussion

Samples of $RMnO_3$, R = Pr, Nd, Tb, Dy, Ho, Er, and Y, have been obtained as black, well-crystallized powders. The excess oxygen content of the Ho, Er, and Y samples is indicated in Table 1. For $YMnO_3$ and $ErMnO_3$ there is a significant Mn^{4+} content, probably inherent to the stabilization of the orthorhombic phase in O_2 flow. For the larger rare-earth perovskites (R = Pr, Nd, Tb, Dy) no oxygen excess has been detected, within the experimental errors. The laboratory XRD diagrams are shown in Figure 1. The patterns are characteristic of strongly distorted perovskites showing sharp, well-defined superstructure reflections. Significant amounts of the competitive hexagonal phase of the same stoichiometry were observed for R = Er, Y. The relative amount of hexagonal phase (Table 1) was subsequently determined from the refinement of the neutron data. The XRD diagrams were indexed in the conventional *Pbnm* orthorhombic model, with unit-cell parameters related to $\mathbf{a}_0$

(24) Rietveld, H. M. *J. Appl. Crystallogr.* **1969**, *2*, 65.
(25) Rodríguez-Carvajal, J. *Physica B* **1993**, *192*, 55.

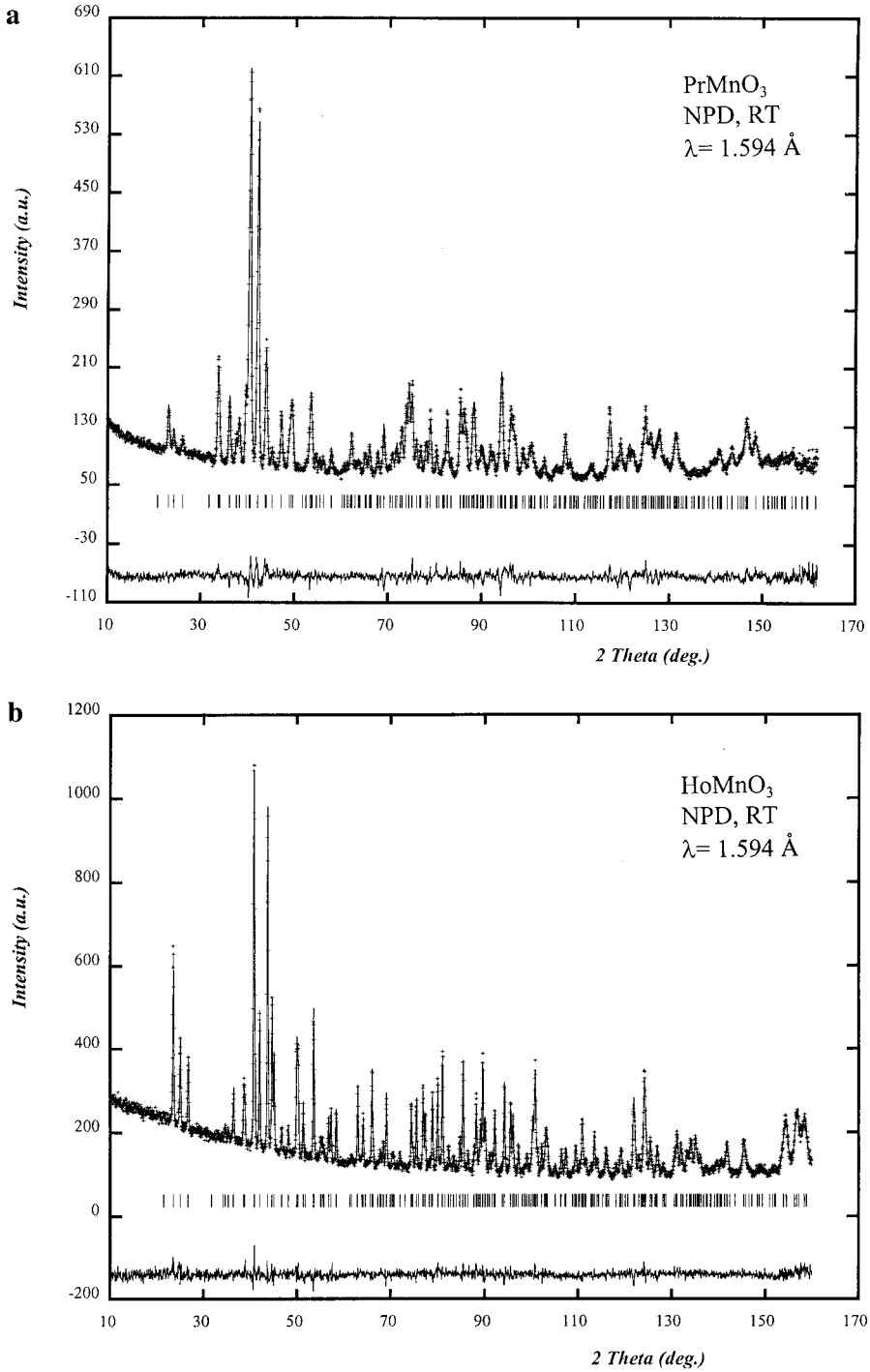

Figure 2. Observed (crosses), calculated (full line), and difference (bottom) NPD Rietveld profiles for $PrMnO_3$ and $HoMnO_3$ ($\lambda = 1.594$ Å). The series of tick marks correspond to the allowed Bragg reflections.

(ideal cubic perovskite, $\mathbf{a}_0 \approx 4$ Å) as $\mathbf{a} \approx \sqrt{2}\mathbf{a}_0$, $\mathbf{b} \approx \sqrt{2}\mathbf{a}_0$, $\mathbf{c} \approx 2\mathbf{a}_0$; Figure 1 illustrates the indexing of the strongly distorted $HoMnO_3$ perovskite. The structural refinement was performed from NPD data using the already reported[15] structural parameters for $LaMnO_3$ as the starting model. The final atomic coordinates, unit-cell parameters, and discrepancy factors for the refinements in the orthorhombic model are given in Table 2. Table 3 contains a selected list of distances and angles. Figure 2 illustrates the goodness of the fit for two representative members of the series, $PrMnO_3$ and $HoMnO_3$. Figure 3 depicts plots of unit-cell dimensions and volume vs the ionic R^{3+} size.[26] The variation of the **b** parameter is very small compared to that of **a** and **c**; this is due to the tilting scheme of MnO_6 octahedra in *Pbnm* perovskites, of the type $a^-a^-c^+$ in Glazer's nomenclature,[27] in which the distortion driven by a reduction of the R^{3+} size leaves **b** almost unchanged. The observed decrease in unit-cell volume scales with the R^{3+} size. The additional contraction observed for Y and Er compounds is related to the slight Mn^{4+} content of these last two perovskites, which will be discussed later. It is worth mentioning that in all cases $\mathbf{c}/\sqrt{2} < \mathbf{a} < \mathbf{b}$. This is characteristic of the so-called O′ structure, and it is originated by the strong cooperative Jahn−Teller effect, inducing an orbital

(26) Shannon, R. D. *Acta Crystallogr. A* **1976**, *32*, 751.

(27) Glazer, A. M. *Acta Crystallogr. B* **1972**, *28*, 3384.

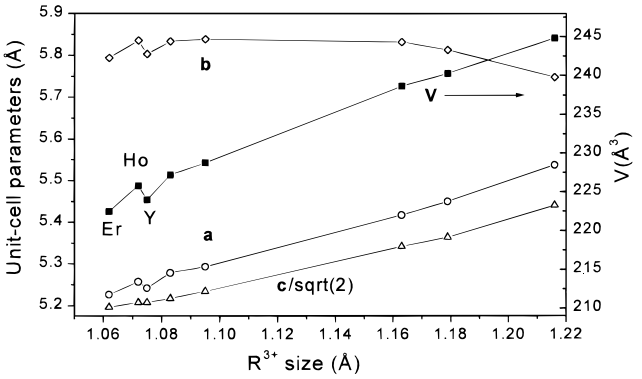

Figure 3. Variation of unit-cell parameters and volume with the R^{3+} ionic radii.[26]

ordering and distorting the MnO_6 octahedra. This is in contrast with the usual situation in perovskites where the primary distorting effect is steric and $\mathbf{c}/\sqrt{2}$ lies between **a** and **b**. It is interesting to note that for $YMnO_3$ and $ErMnO_3$ the presence of Mn^{4+} leads to discontinuities in the **a** and **b** directions, but not in the **c** direction: this implies that the axial Mn−O bonds along the **c** direction (Mn−O1) are not sensitive to the presence of significant amounts of Mn^{4+}, since the JT distortion (perturbed by the Mn^{4+} content) mainly affects the equatorial Mn−O2 bonds, roughly lying on the **ab** plane.

The spontaneous orthorhombic strain, defined as $s = 2(\mathbf{b} - \mathbf{a})/(\mathbf{a} + \mathbf{b})$, progressively increases from R = La to R = Ho perovskites, as shown in Table 2. This parameter not only increases as a consequence of the octahedral tilting but also is a measure of the distortion of the octahedra: both effects are superposed and influence the lattice parameters, together with a more subtle effect due to distortions of the O−Mn−O angles of the octahedron.[28] To evaluate the actual contribution of the JT distortion to the unit-cell-parameter variation, the following approach has been considered: by using the oxygen fractional coordinates and the equations derived by O'Keeffe and Hyde[29] we have determined the magnitude of the octahedral tilt angle and, in turn, the lattice parameters that would be expected in the absence of distortions of the MnO_6 octahedra. Those parameters are listed in Table 4. The strain parameter s' is that expected for undistorted MnO_6 octahedra. Figure 4 plots the s, s' and $s - s'$ variation with the R size. The $s - s'$ difference gives a first evaluation of the evolution of the JT distortion along the series, simply based on the measured unit-cell parameters (and the z(O2) coordinate). A noticeable increase of the JT effect is observed from La to Tb; for smaller rare earths the evolution of $s - s'$ is not significant.

The average Mn−O−Mn angle distortion of the MnO_6 octahedra in $RMnO_3$ can be obtained from the ⟨Mn−O−Mn⟩ bond angle $\langle\theta\rangle$ as $\langle\omega\rangle = 180 - \langle\theta\rangle$. $\langle\omega\rangle$ values for $RMnO_3$ are listed in Table 5. For the sake of comparison, the same calculation has been performed and included for $LaMnO_3$.[15] It is well-known that the presence and magnitude of the octahedral tilting distortions of ABO_3 perovskites can be qualitatively related to the tolerance factor.[30] It would be more enlightening to use 12-coordinate ionic radii of the A-site cations, 6-coordinate radius of the B-site cation, and 2-coordinate radius of oxygen. This approach has the advantage that, if the tolerance factor is greater than or equal to unity, cubic symmetry is expected, on the basis of simple geometric arguments. We have modified this approach by using 9-coordinate radii for the A-site cations because they are more accurately determined for the smaller lanthanides. This is also valid for comparative purposes, although the absolute value of the tolerance factor loses some meaning. Table 5 lists the t_9 tolerance factors, defined as $t_9 = (r_{R9} + r_O)/\sqrt{2}[(r_{Mn} + r_O)]$. The variation of $\langle\omega\rangle$ with t_9 is plotted in Figure 5. A progressive increase of the tilting angle is observed as the tolerance factor decreases.

The variation of Mn−O distances along the series is represented in Figure 6. Although the average ⟨Mn−O⟩ values do not significantly evolve with the R size, individual Mn−O1 (medium) and Mn−O2 (long) bond lengths noticeably diverge for the first terms of the series, from La to Dy. In order to quantify the relative distortion of the octahedra we define the Δ_d parameter, concerning the deviation of Mn−O distances with respect to the average ⟨Mn−O⟩ value, as $\Delta_d = (1/6)\Sigma_{n=1,6}[(d_n - \langle d\rangle)/\langle d\rangle]^2$. For R = La[15] Δ_d is 33.1×10^{-4}; there is a sudden increase of the distortion in the next term of the series, $PrMnO_3$, with $\Delta_d = 43.1 \times 10^{-4}$. From $PrMnO_3$ there is a smooth increase up to $DyMnO_3$, taking a maximum value of $\Delta_d = 49.7 \times 10^{-4}$. Finally, Δ_d progressively decreases down to 43.0×10^{-4} for $ErMnO_3$. Again, we think that this unexpected decrease of the octahedra distortion can be due to the presence of significant amounts of Mn^{4+} in Er and Y perovskites, as shown in Table 1. It should be recalled that these perovskites were prepared in an O_2 flow as the only way to minimize the formation of the competitive hexagonal phases. In fact, perhaps the presence of a minor Mn^{4+} content favors the stabilization of the perovskite phase for the last, very distorted terms of the $RMnO_3$ series, as suggested by Brinks et al.[22] Note that the introduction of some Mn^{4+} (smaller in size than Mn^{3+}) would lead to an increase of the tolerance factor, thus stabilizing the structure.

In Table 5 we have also included some geometrical parameters directly related to the JT effect. The breaking of the degeneracy of e_g orbitals can be described by the coefficients c_1 and c_2 determining the orbital occupation. The bonding (ψ_g) and antibonding (ψ_e) orbitals are obtained as the linear combinations $\psi_g = c_1\varnothing_{x^2-y^2} + c_2\varnothing_{z^2}$ and $\psi_e = c_2\varnothing_{x^2-y^2} - c_1\varnothing_{z^2}$. The local modes characterizing the JT effect are defined as $Q_2 = 2(l - s)/\sqrt{2}$ and $Q_3 = 2(2m - l - s)/\sqrt{6}$, where m, l, and s stand for medium, long, and short Mn−O distances. Finally, the coefficients c_1 and c_2 ($c_1^2 + c_2^2 = 1$) can be obtained from the relations $\tan\varphi = Q_2/Q_3$ and $\tan(\varphi/2) = c_1/c_2$ (see refs 31, 32).

Figure 5 includes the variation of c_1 with the R^{3+} size. The orbital ordering associated with the JT effect experiences a variation similar to that already described for the residual strain ($s - s'$) and the distortion parameter Δ_d: a progressive decrease of the c_1 parameter is observed, reaching a plateau for the last terms of the series. The fact that the anisotropy of the Mn−O bonds seems to increase from La to Tb can be explained by the progressive reduction of the covalent contribution of Mn−O bonds, which in turn is due to the reduction of the electropositive character from La to Tb. For the smaller rare-earth cations the magnitude of the orbital ordering reaches a plateau, probably because this is the maximum distortion that the stabilization of e_g electrons can induce on the crystal structure for this particular system; moreover, for Er and Y the presence of some Mn^{4+}

(28) Woodward, P. M.; Vogt, T.; Cox, D. E.; Arulraj, A.; Rao, C. N. R.; Karen, P.; Cheetham, A. K. *Chem. Mater.* **1998**, *10*, 3652.
(29) O'Keeffe, M.; Hyde, B. G. *Acta Crystallogr. B* **1977**, *33*, 3802.
(30) Goodenough, J. B.; Longo, J. M. In *Magnetic and Other Properties in Oxides and Related Compounds*; Hellwege, K. H., Hellwege, A. M., Eds.; Springer-Verlag: Berlin, 1970. Landolt-Börnstein, New Series, Group III, Vol. 4a, Chapter 3, p 126.
(31) Matsumoto, G. *J. Phys. Soc. Jpn.* **1970**, *29*, 606.
(32) Kanamori, J. *J. Appl. Phys.* **1960**, *31*, 14S.

Table 3. Main Bond Distances (Å) and Selected Angles (deg) for Orthorhombic $RMnO_3$ (R = La, Pr, Nd, Tb, Dy, Ho, Y, Er) Perovskites at 295 K[a]

		La	Pr	Nd	Tb	Dy	Ho	Y	Er
					MnO_6 Octahedra				
Mn−O1 (x2)	*m*	1.9680(3)	1.9530(5)	1.9514(7)	1.9401(7)	1.9437(6)	1.9435(7)	1.9385(15)	1.9382(13)
Mn−O2 (x2)	*l*	2.178(1)	2.2100(16)	2.218(2)	2.221(2)	2.2238(15)	2.2224(17)	2.200(4)	2.199(3)
Mn−O2 (x2)	*s*	1.907(1)	1.9087(16)	1.905(2)	1.905(2)	1.9030(14)	1.9046(16)	1.904(4)	1.903(3)
⟨Mn−O⟩		2.0178(4)	2.0239(6)	2.0248(7)	2.022(1)	2.0235(13)	2.0235(13)	2.014(3)	2.013(2)
$10^4\Delta_d$		33.1	43.1	46.4	48.9	49.7	48.9	43.1	43.0
Mn−O1−Mn (x2)		155.48(2)	152.36(2)	150.86(3)	145.06(3)	143.23(2)	142.47(3)	143.51(6)	142.82(5)
Mn−O2−Mn (x4)		155.11(5)	150.51(6)	149.63(8)	145.36(7)	144.70(6)	144.08(6)	144.55(15)	143.92(12)
⟨Mn−O−Mn⟩		155.23(3)	151.13(3)	150.04(6)	145.26(4)	144.21(4)	143.54(5)	144.20(13)	143.55(9)
					RO_9 Polyhedra				
R−	O1	2.560(2)	2.482(4)	2.463(4)	2.333(3)	2.325(2)	2.309(3)	2.306(6)	2.305(5)
R−	O1	2.425(2)	2.367(4)	2.351(4)	2.289(3)	2.262(2)	2.250(3)	2.252(6)	2.225(5)
R−	$O1_{(long)}$	3.158(2)	3.166(4)	3.164(4)	3.179(3)	3.201(3)	3.205(3)	3.176(6)	3.186(5)
R−	O2 (x2)	2.650(2)	2.626(3)	2.602(3)	2.526(2)	2.522(2)	2.512(2)	2.501(5)	2.500(4)
R−	O2 (x2)	2.459(2)	2.404(3)	2.387(3)	2.321(2)	2.303(2)	2.293(3)	2.303(5)	2.284(4)
R−	O2 (x2)	2.698(2)	2.628(3)	2.628(3)	2.572(2)	2.567(2)	2.564(2)	2.553(4)	2.558(4)
$\langle R-O\rangle_{(8\ short)}$		2.575(2)	2.521(3)	2.506(3)	2.433(2)	2.421(2)	2.412(2)	2.409(5)	2.402(4)

[a] *m*, *l*, and *s* stand for medium, large, and short Mn−O distances. The distortion parameter Δ_d for NiO_6 octahedra with an average Mn−O distance $\langle d\rangle$ is defined as $\Delta_d = (1/6)\sum_{n=1,6}[(d_n - \langle d\rangle)/\langle d\rangle]^2$. Data for La are taken from ref 15.

Table 4. Calculated Tilting Angle (deg) and Unit-Cell Parameters (Å) Considering Undistorted MnO_6 Octahedra[a]

R	φ[b]	a[c]	b	c	s'
La	15.24	5.444	5.577	7.790	0.024
Pr	17.06	5.394	5.561	7.741	0.030
Nd	17.85	5.371	5.553	7.717	0.033
Tb	20.23	5.295	5.529	7.641	0.043
Dy	20.66	5.280	5.524	7.627	0.045
Y	20.62	5.281	5.525	7.628	0.045
Ho	21.18	5.262	5.519	7.608	0.048
Er	21.49	5.250	5.515	7.597	0.049

[a] The strain parameter is defined as $s' = 2(b - a)/(a + b)$. [b] $\varphi = -\sqrt{48}\ \arctan[z(O2)]$ (ref 29). [c] $a = d\sqrt{8}\cos\varphi$; $b = d[8(2 + \cos^2\varphi)/3]^{1/2}$; $c = d[48/(1 + \sec^2\varphi)]^{1/2}$ (ref 29); $d = 1.995$ Å (sum of ionic radii for Mn^{3+} and O^{2-}, ref 26).

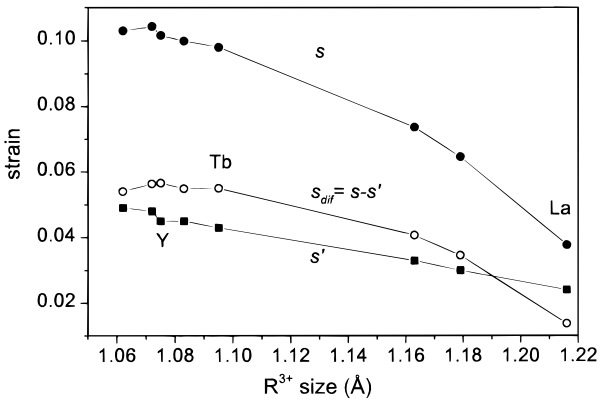

Figure 4. Evolution of the observed strain (*s*), the calculated strain for undistorted MnO_6 octahedra (*s*′), and the difference between both parameters, $s - s'$, with the R^{3+} ionic radius.[26]

certainly inhibits a further increase. This behavior is similar to that found for $RNiO_3$ perovskites, containing Ni^{3+}.[33,34] This cation is also a JT ion with a single electron in an orbitally degenerate ground state ($t^6_{2g}e^1_g$). In the $RNiO_3$ series no anisotropy could be detected in the NiO_6 octahedra for the

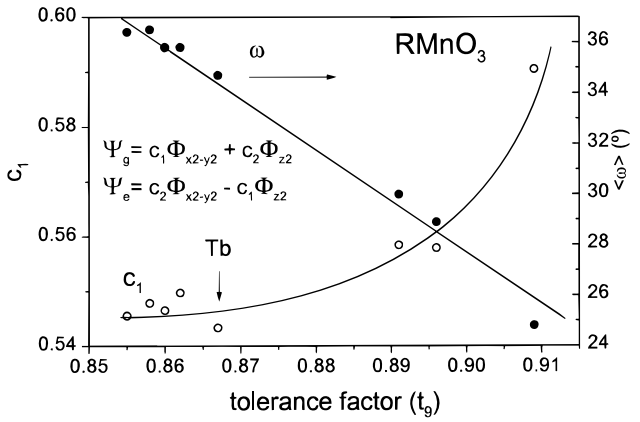

Figure 5. Variation of the c_1 mixing coefficient and average Mn−O−Mn angle distortion of the octahedra as a function of the tolerance factor (t_9) of the perovskite structure.

Table 5. Geometrical Parameters Characterizing the Distortion of $RMnO_3$ Perovskites: Tolerance t_9 Factor, Mean Tilting Angles of MnO_6 Octahedra (deg), c_1 and c_2 Coefficients as Defined in the Text

R	t_9	$\langle\omega\rangle$	c_1	c_2
La	0.909	24.8	0.5905	0.8070
Pr	0.896	28.9	0.5579	0.8299
Nd	0.891	30.0	0.5584	0.8296
Tb	0.867	34.7	0.5433	0.8395
Dy	0.862	35.8	0.5497	0.8354
Y	0.860	35.8	0.5465	0.8375
Ho	0.858	36.5	0.5478	0.8366
Er	0.855	36.4	0.5455	0.8381

largest rare-earth cations (R = La, Pr, Nd), given the strongly covalent character of the Ni−O bonds;[35] however, the last terms of the series show an increased anisotropy of NiO_6 octahedra,[33,34] as a consequence of the manifestation of JT-induced distortions. These distortions are, for this particular system, much smaller (by 1 order of magnitude) than those observed in the $RMnO_3$ series.

The calculation of the valence of the cations and anions present in the solid, following Brown's bond-valence model,[36,37]

(33) Alonso, J. A.; García-Muñoz, J. L.; Fernández-Díaz, M. T.; Aranda, M. A. G.; Martínez-Lope, M. J.; Casais, M. T. *Phys. Rev. Lett.* **1999**, *82*, 3871.

(34) Alonso, J. A.; Martínez-Lope, M. J.; Casais, M. T.; Aranda, M. A. G.; Fernández-Díaz, M. T. *J. Am. Chem. Soc.* **1999**, *121*, 4754.

(35) García-Muñoz, J. L.; Rodríguez-Carvajal, J.; Lacorre, P.; Torrance, J. B. *Phys. Rev. B* **1992**, *46*, 4414.

Table 6. Valences Determined from the Bond-Valence Model[a] for R, Mn, and O within the RO_8 and MnO_6 Coordination Polyhedra in $RMnO_3$ Perovskites[b]

	La	Pr	Nd	Tb	Dy	Ho	Y	Er
R	2.909(5)	2.949(10)	2.931(9)	2.984(8)	2.988(5)	2.964(7)	2.898(16)	2.952(13)
Mn	3.132(3)	3.118(5)	3.124(6)	3.156(5)	3.147(4)	3.144(5)	3.200(11)	3.206(9)
O1	1.994(4)	2.113(7)	2.115(7)	2.217(6)	2.220(4)	2.221(5)	2.214(12)	2.246(11)
O2	1.973(4)	1.977(6)	1.970(6)	1.961(5)	1.958(4)	1.944(5)	1.942(10)	1.956(9)
GII	0.117	0.086	0.093	0.135	0.134	0.136	0.158	0.168

[a] The valence is the sum of the individual bond valences (s_i) for R−O and Mn−O bonds. Bond valences are calculated as $s_i = \exp[(r_0 - r_i)/B]$; $B = 0.37$, $r_0 = 1.760$ for the $Mn^{3+}-O^{2-}$ pair; for the $R^{3+}-O^{2-}$ pairs, for La, Pr, Nd, Tb, Dy, Ho, Y, Er, $r_0 = 2.172$, 2.135, 2.117, 2.049, 2.036, 2.023, 2.014, 2.010, from ref 37. Individual R−O and Mn−O distances (r_i) are taken from Table 3. The global instability index (GII) is calculated as the root mean of the valence deviations for the $j = 1...N$ atoms in the asymmetric unit, according to $GII = (\sum_j[\sum_i(s_{ij} - V_j)^2]/N)^{1/2}$. [b] For $LaMnO_3$ valences are calculated from structural data given in ref 15.

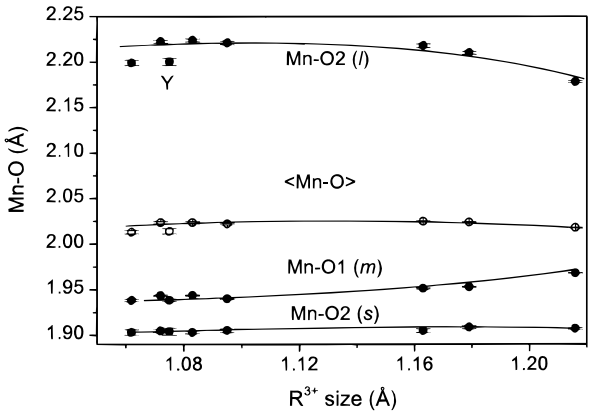

Figure 6. Evolution of the Mn−O bond lengths along the $RMnO_3$ series. *l*, *m*, and *s* stand for long, medium, and short bonds, as defined in Table 3.

is also enlightening. This model gives a phenomenological relationship between the formal valence of a bond and the corresponding bond length. In ideal nonstrained structures, the bond-valence-sum (BVS) rule states that the formal charge of the cation (anion) is equal to the sum of the bond valences around this cation (anion). This rule is satisfied only if the stress introduced by the coexistence of different structural units can be relieved by the existence of enough degrees of freedom in the crystallographic structure. The departure of the BVS rule is a measure of the existing stress in the bonds of the structure. The overall stress can be quantified by means of a global instability index (GII),[38] calculated as the root mean of the valence deviations for the $j = 1...N$ atoms in the asymmetric unit, according to $GII = (\Sigma_j[\Sigma_i(s_{ij} - V_j)^2]/N)^{1/2}$.

Table 6 lists the valences calculated for R, Mn, and O atoms from the individual R−O and Mn−O bond distances of Table 3, as well as GII values. Mn atoms exhibit valences somewhat higher than the expected value of +3; probably this method overestimates them. However, it is interesting to observe the relative variation along the series: for Er and Y oxides, Mn cations exhibit a valence significantly higher than that found in the remaining perovskites. This is in agreement with the oxidation state measurements obtained by thermal analysis. The progressive deviation of the valences for the last terms of the series implies an increasing structural metastable character, as shown by the very quick increase of the corresponding GII values, reaching 0.168 for $ErMnO_3$. Actually, crystal structures with GII higher than 0.1 are usually considered as seriously strained, which explains the difficulties found in the synthesis of the last members of the $RMnO_3$ perovskite family, and the challenges presented by the preparation of isostructural compounds for R^{3+} smaller than Er^{3+}.

Conclusions

In summary, the presence of a primary electronic effect responsible for static orbital ordering is patent in all members of the $RMnO_3$ series. This effect significantly increases from La to Tb and then remains essentially unchanged for the last members of the family (R = Dy, Ho, Er, Y). The electron−lattice interaction is, for sufficiently small R^{3+} cations, considerably stronger than that found for $LaMnO_3$, as a manifestation of the more ionic character of the perovskites with smaller R. Independently, a simple steric factor accounts for the increase of the global distortion of the perovskite structure, as far as the degree of tilting of the MnO_6 octahedra is concerned. A progressive increment of the average tilt angle is observed from $LaMnO_3$ to $ErMnO_3$, this last oxide showing a minimum tolerance factor of $t_9 = 0.855$.

Acknowledgment. The authors would like to thank the ILL for making available the beam time and financial support by the Spanish CYCyT for funding the PB97-1181 project.

IC990921E

(36) Brown, I. D. In *Structure and Bonding in Crystals;* O'Keeffe, M., Navrotsky, A., Eds.; Academic Press: New York, 1981; Vol. *2*, pp 1−30.

(37) Brese, N. E.; O'Keeffe, M. *Acta Crystallogr. Sect. B* **1991**, *47*, 192.

(38) Brown, I. D. *Z. Kristallogr.* **1992**, *199*, 255.